Gravity-capillary internal wave simulation using a binary fluid lattice Boltzmann model

J. M. Buick[1], J. A. Cosgrove[2] and C. A. Greated[2]

1) Physics and Electronics

School of Biological, Biomedical and Molecular Sciences

University of New England

NSW 2351, Australia.

2) Department of Physics and Astronomy

The University of Edinburgh

The Kings Buildings, Mayfield Road

Edinburgh EH9 3JZ, Scotland, U.K.

June 20, 2003

Abstract

The simulation of internal waves using a lattice Boltzmann model is considered. Two different situations are considered: a sharp interface between two fluids of different densities; and a continuous density change over a finite depth. Both situations are examined for pure gravity waves and for gravity-capillary driven waves. When a sharp interface is

applied the waves motion is that of interfacial waves. When a wide interface is applied interfacial waves are simulated when surface tension effects are significant. When the surface tension effects are small enough that they can be neglected, internal waves on a continuously varying density distribution are modelled.

Keywords: lattice Boltzmann, internal waves, gravity waves, capillary waves.

1 Introduction

The lattice Boltzmann model (LBM) [1] has been developed over recent years as an alternative to traditional computational fluid mechanics. The underlying concept of the LBM is to incorporate the fundamental physics of the problem into a simplified kinetic equation such that the correct macroscopic behaviour of the fluid is recovered. Using this approach a single phase LBM can be derived which macroscopically satisfies the continuity and Navier-Stokes equations for an incompressible fluid [2]. The approach of including the underlying physics into the Boltzmann equation has enabled the LBM to be used to simulate more complex fluid systems. Examples of this include the simulation of binary fluids [3, 4], a model which is applied in the work presented here. This model simulates an immiscible, binary fluid mixture based on the Cahn-Hilliard approach to non-equilibrium dynamics. The physical basis of this model ensures that the simulation is thermodynamically consistent. Extensions of this approach have lead to LBM models for ternary fluid mixtures such as an oil-water-surfactant system [5]. Alternative approaches to modelling multi-phase [6] and ternary [7] within a LBM framework have also been considered by simulating an interaction force between nearest neighbours. This approach has been further investigated by Martys and Douglas [8] who consider a direct comparison between the LBM simulations and the properties of real fluids. This was

done by considering a reduced set of parameters which were largely independent of the model parameters. This enabled a better comparison to be made between the LBM model and other models as well as experiments. Such a comparison indicated that the LBM corresponds to an ideal mean-field fluid over a broad range. Unfortunately Martys and Douglas [8] did not consider the Binary fluid model applied here, however its derivation based on the Cahn-Hilliard model suggests it is a realistic approach.

Internal waves occur in two situations: when there is a sharp density change between two layers of different fluids; and when there is a region of density variation within a fluid, such as is commonly found in the ocean, for example at a thermocline. Internal waves are most commonly observed in shallow, coastal areas such as straits, marginal seas, continental shelfs and fjords [9, 10, 11, 12], but have also been observed in deep oceans [13, 14]. Internal waves in the ocean can have significant influence marine activities such as oil drilling [15], and are thought to redistribute zooplankton, nutrients and other particulate substances [10] and consequently influence the movement and feeding habits of marine animals [15].

It has recently been shown [16, 17] that an LBM of a binary fluid mixture [3, 4] can be used to simulate internal gravity waves. The technique has been used to simulate pure gravity waves at a sharp interface between two fluids [16], such as the interface between fresh and salt water, and at a continuous but finite density change [17], such as is commonly found at a thermocline. In this paper both cases of internal waves are considered in the regimes of pure gravity waves and gravity-capillary waves. The motion of gravity-capillary waves is significantly influenced by both gravity and surface tension forces. These waves have wavelengths in the intermediate range between short wavelengths, at which surface tension forces are solely responsible for driving the motion, and

the longer wavelengths where surface tension forces are negligible compared to gravity. The range of wavelengths for which gravity and surface tension forces are of the same order depends on the relative density of the two fluids as well as the particular fluids which are in contact at the interface. For example, interfacial waves between a layer of oil and fresh water may be significantly influenced by surface tension forces, while a wave with the same wavelength, propagating between fresh water and a saline solution, will behave differently. In this paper we investigate the ability of this LBM to simulate gravity-capillary internal waves as well as pure gravity waves. Further, the investigation is extended to consider interfaces corresponding to a sharp density step and to a continuous density variation for both types of waves - a feature which has not been investigated previously for this type of model.

An alternative to the LBM approach to simulating fluid interfaces is the Ghost Fluid Method (GFM) [18]. This simulation approach incorporates the best properties of Eulerian schemes which perform well away from material interfaces, and Lagrangian schemes which work well at material interfaces. The GFM has been applied to a wide range of problems including simulating interphases involving a chemical reaction between the constituent fluids [19] such as combustion or evaporation. The GFM differs from the LBM in a number of ways. Firstly the GFM uses traditional computational fluid mechanics techniques such as the Runge-Kutta method to solve the basic fluid equations. Secondly, the GFM describes the fluid by an Euler equation in contrast the the LBM in which the simulated fluid satisfy the Navier-Stokes equation including viscous dissipation. Thirdly, possible the greatest difference between the techniques is that the GFM model has been designed is simulate compressible gas flow with large density variations, while the LBM model generally simulated incompressible fluids where density variations are minimal. It is clear, therefore, that although both techniques can be applied to simulate

fluid interfaces, they have both been developed to simulated different flow regimes. LBM simulations of a compressible gas satisfying the Euler equation have been reported [20], however the simulation of multi-phase compressible simulations have not been considered.

2 The binary fluid lattice Boltzmann model

Here we employ a binary fluid model [3, 4] which simulates two immiscible fluids which, in the presence of gravity [16, 21], can have different potential densities. The simulations are performed on a hexagonal grid with the unit link vectors given by $\boldsymbol{e}_i = \sin(\frac{\pi i}{3} - \frac{\pi}{6})\boldsymbol{i} + \cos(\frac{\pi i}{3} - \frac{\pi}{6})\boldsymbol{k}, i = 1, 2, ..., 6$ where $\boldsymbol{i}$ and $\boldsymbol{j}$ are orthogonal unit vectors in the horizontal and vertical directions respectively and $\boldsymbol{e}_0$ is the null vector. The system is described in terms of the total density of both fluids, $\rho(\boldsymbol{r}, t)$, and the order parameter, $d(\boldsymbol{r}, t)$, which determines which fluid is present or, at the interface, the proportions of each fluid. These are found from the distribution functions f_i and h_i as $\rho = \sum_i f_i$ and $d = \sum_i h_i$ while the fluid velocity, $\boldsymbol{u}$, is given by $\rho\boldsymbol{u} = \sum_i f_i \boldsymbol{e}_i$. The two distribution functions are simulated directly using two Boltzmann equations:

$$f_i(\boldsymbol{r} + \boldsymbol{e}_i, t + 1) - f_i(\boldsymbol{r}, t) = -\frac{1}{\tau_\rho}(f_i - \overline{f_i}) + \frac{1}{3}F_\alpha e_{i\alpha} \tag{1}$$

and

$$h_i(\boldsymbol{r} + \boldsymbol{e}_i, t + 1) - h_i(\boldsymbol{r}, t) = -\frac{1}{\tau_d}(h_i - \overline{h_i}), \tag{2}$$

where Roman indices are used as labels and Greek indices are used to represent vector components with summation over repeated Greek indices assumed. The left-hand-side of equations (1) and (2) represent the streaming of f_i and h_i respectively on the computational grid. The right-hand side represents the relaxation of f_i and h_i toward their equilibrium values $\overline{f_i}$ and $\overline{h_i}$. The rate at which the distribution functions relax is deter-

mined by the two relaxation times: τ_ρ for the f_i and τ_d for the h_i. The body force $\boldsymbol{F}$ and the equilibrium distribution functions $\overline{f_i}$ and $\overline{h_i}$ are given by

$$\boldsymbol{F} = \rho g = [g_a(\rho - d) + g_b(\rho + d)]\boldsymbol{k}, \tag{3}$$

$$\overline{f}_i = A + Bu_\alpha e_{i\alpha} + Cu^2 + Du_\alpha u_\beta e_{i\alpha} e_{i\beta} + G_{\alpha\beta} e_{i\alpha} e_{i\beta}, \quad i = 1, ..., 6, \tag{4}$$

$$\overline{f}_0 = A_0 + C_0 u^2, \tag{5}$$

$$\overline{h}_i = H + Ku_\alpha e_{i\alpha} + Ju^2 + Qu_\alpha u_\beta e_{i\alpha} e_{i\beta}, \quad i = 1, ..., 6 \tag{6}$$

and

$$\overline{h}_0 = H_0 + J_0 u^2, \tag{7}$$

where $\boldsymbol{k}$ is a unit vector in the vertical direction. The form of Eqs. (4) and (5) is common to any LBM simulation and insures that the accuracy of the simulation is second order in the velocity. The coefficients $A, A_0, ..., G_{\alpha\beta}$ are determined so that local mass and momentum are conserved. Similarly, Eqs. (6) and (7) are common to any two-fluid simulation and the local conservation of the individual fluid densities is used to determine the coefficients. In the binary fluid model employed here further constraints are imposed on the coefficients of Eqs. (4)–(7) [3, 4]:

$$\sum_i \overline{f}_i e_{i\alpha} e_{i\beta} = P_{\alpha\beta} + \rho u_\alpha u_\beta \tag{8}$$

and

$$\sum_i \overline{h}_i e_{i\alpha} e_{i\beta} = \Gamma \Delta\mu \delta_{\alpha\beta} + d u_\alpha u_\beta, \tag{9}$$

where Γ is the fluid mobility. The from of the pressure tensor, $P_{\alpha\beta}$, and the chemical potential, $\Delta\mu$, are found from the free energy of two ideal gases with a repulsive interaction

energy [3] and are

$$P_{\alpha\beta} = \left[\rho T - \frac{\kappa}{2}\left(\rho\nabla^2\rho + d\nabla^2 d + |\nabla\rho|^2 + |\nabla d|^2\right)\right]\delta_{\alpha\beta} + \kappa\left(\partial_\alpha\rho\partial_\beta\rho + \partial_\alpha d\partial_\beta d\right) \tag{10}$$

and

$$\Delta\mu = -\frac{\Lambda}{2}\frac{d}{\rho} + \frac{T}{2}\log\left(\frac{1+d/\rho}{1-d/\rho}\right) - \kappa\nabla^2 d. \tag{11}$$

For these conditions the coefficients can be found as

$$A = (\rho T - \kappa d\nabla^2 d/2 - \kappa\rho\nabla^2\rho/2)/3, \qquad B = \rho/3, \qquad C = -\rho/6,$$

$$D = 2\rho/3, \qquad G_{xy} = G_{yx} = \frac{2\kappa}{3}\left[\frac{\partial\rho}{\partial x}\frac{\partial\rho}{\partial y} + \frac{\partial d}{\partial x}\frac{\partial d}{\partial y}\right],$$

$$G_{xx} = -G_{yy} = \frac{\kappa}{3}\left[\left(\frac{\partial\rho}{\partial x}\right)^2 - \left(\frac{\partial\rho}{\partial y}\right)^2 + \left(\frac{\partial d}{\partial x}\right)^2 - \left(\frac{\partial d}{\partial y}\right)^2\right], \tag{12}$$

$$H = \Gamma\Delta\mu/3, \qquad K = d/3, \qquad J = -d/6, \qquad Q = 2d/3,$$

$$A_0 = \rho - 6A, \qquad C_0 = -\rho, \qquad H_0 = d - 6H, \qquad J_0 = -d.$$

The interfacial energy, κ, and the gravitational terms, g_a and g_b, are free to be varied to change the properties of the binary fluid. The interfacial energy, κ, affects the thickness of the interface and the surface tension between the two fluids and is varied in the simulations to give the required interfacial properties. The gravitational terms, g_a and g_b, affect the relative density of the fluids [16]. The relative density of the two fluids, $f > 1$, defined as the density of the heavier fluid divided by the density of the lighter fluid is given by $f = g_2/g_1$, where

$$g_1 = \frac{3g_a + g_b}{4} \quad \text{and} \quad g_2 = \frac{g_a + 3g_b}{4}, \tag{13}$$

for $g_a < g_b$, while the acceleration due to gravity, g, is given by

$$g = \frac{g_1 + g_2}{2}. \tag{14}$$

The temperature, T, the interaction strength parameter, Λ, the mobility, Γ, and the relaxation times, τ_ρ and τ_d, are also free to be varied, however in the simulations presented here their values were fixed. The value of λ was set to 1.1, following Orlandini *et al.* [3]. This defines a critical temperature $T_c = \lambda/2$ such that for $T > T_c$ a homogeneous mixture of the two components is simulated and for $T < T_c$ the fluid phase separates into two distinct phases. We therefore require $T < T_c$ for an immiscible binary fluid and select $T = 0.5$ which gives $d/\rho \simeq 0.5$. As T is decreased from T_c the value of d/ρ increases as the composition of the two phases changes. The fluid viscosity is a function of τ_ρ and is given by [4]

$$\nu = \frac{2\tau_\rho - 1}{8}. \tag{15}$$

The value of the relaxation time τ_ρ can be selected to determine the fluid viscosity and can be varied to change, for example, the Reynolds number of the simulation; subject to the condition $\tau_\rho > 1/2$, required so that f_i relaxes toward $\overline{f}_i$ in equation (1) and to give a positive viscosity. In practice the model is found to become unstable for small τ [22], here $\tau_\rho = 0.7$ was used. The other relaxation time τ_d is also subject to $\tau_d > 1/2$ (see equation (2)) and, along with Γ determined the diffusion constant for the binary fluid [3]. Since we are considering the binary fluid in its immiscible state we select $\Gamma = 0.1$ and determine τ_d from other considerations. In a LBM scheme the continuity and Navier-Stokes equation, and when a multi-component fluid is considered the convection-diffusion equation, are derived from the Boltzmann equation by first performing a Taylor expansion and neglecting higher-order terms in the discrete time step (which must be small with

respect to the typical time-scale of the simulation). If the next order terms are included in the expansion the desires continuum equations are derived with erroneous extra terms. For the binary fluid model considered here, these terms are zero for $\tau_d = 0.789$ [3, 4]. This is the value used in the simulations presented here. These higher-order terms can lead to spurious velocities in the interface region for the binary fluid model, however, these are minimised by the choice of τ_d [4].

Equations (1) and (2) are the lattice Boltzmann equations which describe the evolution of the system. They also define the lattice units, namely the lattice space, $|\boldsymbol{e}_i| = 1$, and the time step, $\Delta t = 1$. These units are used to measure quantities from the simulation. For example, $\lambda = 256$ corresponds to a wavelength of 256 lattice spaces and $g_a = 0.0001$ is measured in units of lattice spaces (time steps)$^{-2}$. Dimensionless quantities such as the relative fluid density, f, or the Reynolds or Froude number of the wave must be used when comparing the simulations to a real life situation.

3 The interfacial energy

The binary fluid model simulates two immiscible fluids separated by an interface. The form of the interface and the surface tension between the fluids is determined by the value of the interfacial energy κ (when all other model parameters are fixed). This is shown for two values of κ in figures 1 and 2 which show the total density, ρ, and the order parameter, d, plotted against the x-position along a line through the centre of a circular bubble of one fluid inside the other in the absence of gravity. The centre of the bubble is at $x = 32$. Figure 1 shows a small drop in the fluid density at the interface of no more than 0.5 %. This change is smaller when $\kappa = 0.001$ and the interface is sharper. It also shows that the density is slightly different inside and outside the bubble, the density change is largest when $\kappa = 0.1$. Figure 2 shows the change in the order parameter. When

$\kappa = 0.001$ the interface is sharp, no larger than one lattice spacing. There is a smooth, more gradual, change when $\kappa = 0.1$, the width of the interface can be seen in figure 2 to be approximately 10. We can see from figure 2 that, for the parameters used here, the two fluids are described by $d \simeq \pm 1/2$. These descriptions of the interface are in agreement with other observations [4] and figure 2 also contains a curve for $\kappa = 0.2$ to enable a direct comparison. The results presented in figure 1 show a density difference across the interface of 3.5×10^{-5} and 1.9×10^{-3} for $\kappa = 0.001$ and $\kappa = 0.1$ respectively. From this the surface tension, σ, across the interface can be calculated using the Laplace law, $\sigma = \Delta p r$, where Δp is the pressure change across the interface found from the density change multiplied by the temperature and r is the radius of the bubble defined to be the distance between the centre of the bubble ($x = 32$) and the point where $d = 0$. This gives $\sigma = 3.4 \times 10^{-4}$ when $\kappa = 0.001$ and $\sigma = 1.8 \times 10^{-2}$ when $\kappa = 0.1$.

4 The frequency of internal waves

Gravity wave motion between immiscible, homogeneous, incompressible fluids can, provided any disturbances are small, be described by linear wave theory in a manner analogous to linear surface waves [23, 24]. Consider two fluids of depth h_1 and h_2 with densities ρ_1 and ρ_2, $\rho_1 < \rho_2$, separated by a sharp interface. Let the origin be at the interface with the x-coordinate horizontal and the z-coordinate vertically upwards. If the interface is far from the bed and the free surface so that $\tanh(kh_1) \simeq 1$ and $\tanh(kh_2) \simeq 1$ and surface tension effects are negligible then the wavenumber k and the frequency ω_o are related in a form analogous to the dispersion relation for surface waves:

$$\omega_0^2 = g'k \tag{16}$$

where g' is the reduced gravity and is defined by

$$g' \stackrel{\text{def}}{=} \frac{(f-1)}{(f+1)} g, \tag{17}$$

g is the acceleration due to gravity and $f = \rho_2/\rho_1$ is the relative density of the two fluids. If, however, surface tension is not negligible the frequency is given by [25]

$$\omega_\sigma^2 = g'k + \frac{k^3\sigma}{\rho(f+1)}, \tag{18}$$

where σ is the surface tension. If both fluids have viscosity ν then the wave frequency is reduced by an amount ω'. To $O(\nu)$ the value of ω' is given by [26]

$$\omega' = (\omega_0)^{1/2} \frac{\sqrt{2}kf\sqrt{\nu}}{(1+f)^2}. \tag{19}$$

Thus, for a two-layer model the frequency, ω_2, of an interfacial wave between two viscous fluids is, to order $O(\nu)$,

$$\omega_2 = \omega_\sigma - \omega'. \tag{20}$$

If the wavelength of the wave is such that $\lambda > 3\lambda_m$, where [25]

$$\lambda_m = 2\pi\sqrt{\frac{\sigma}{\rho(f-1)g}} \tag{21}$$

then the influence of surface tension on the wave frequency will not exceed 5 % and the wave can be considered as being a pure gravity wave in which case $\omega_2 \simeq \omega_0 - \omega'$. In some situations the two-fluid model may have some shortcomings since there can be a small, but finite, region around the interface where the density changes smoothly from ρ_1 to ρ_2. In this case an incompressible, irrotational and homogeneous fluid satisfying the

Boussinesq approximation is described by the Sturm-Liouville equation [27]

$$\frac{\mathrm{d}}{\mathrm{d}z}\left[P(z)\frac{\mathrm{d}\mathcal{W}(z)}{\mathrm{d}z}\right] + \left[Q(z) + ER(z)\right]\mathcal{W}(z) = 0, \tag{22}$$

where $P(z) = 1$, $Q(z) = -k^2$, $E = 1/c^2$ where $c = \omega/k$ is the wave celerity and $R(z) = N^2(z)$ where $N(z)$ is the Brunt-Väisälä frequency,

$$N^2(z) = -\frac{g}{\rho}\frac{\partial \rho}{\partial z}. \tag{23}$$

Equation (22) can not, in general, be solved analytically. It is known [28], however, that, provided $P(z) > 0$, $Q(z) \leq 0$ and $R(z) > 0$, the Sturm-Liouville equation has an infinite number of real, positive Eigen-value solutions, E_n, n=0, 1, 2, ..., each with a corresponding Eigen-functions $\mathcal{W}_n$ having n+1 extremes in the z-range in which ρ is defined. For each mode (n=0, 1, ...) there is a unique relationship between the celerity $c = \sqrt{1/E_n}$ and the wave number k. This relationship is referred to as the dispersion relation of that mode. The $n = 0$ mode corresponds to the two-fluid solution and tends to it as the density distribution, $\rho(z)$, approaches a step function at the interface. For this node we can define $\omega_c = \sqrt{1/E_0}k$ where the density distribution is given by

$$\rho(z) = \begin{cases} \rho_2 & z < -\dfrac{l}{2} \\ \dfrac{(\rho_1 - \rho_2)z}{l} + \dfrac{\rho_1 + \rho_2}{2} & -\dfrac{l}{2} \leq z \leq \dfrac{l}{2} \\ \rho_1 & z > \dfrac{l}{2} \end{cases} . \tag{24}$$

This gives the frequency of a wave on a density distribution which varies uniformly between two densities ρ_1 and ρ_2 over a depth l. Here there is no consideration of the

viscous nature of a real fluid. As with the two-layer model we expect that the viscous nature of the fluid will only be evident in boundary layers which for a single fluid occur at the upper and lower boundaries. Provided these boundaries are far from the fluid motion they will have a negligible effect on the motion. This is in contrast to the two-layer model where the frequency is altered due to a boundary layer forming at the interface.

5 Applicability of the theoretical models to the lattice Boltzmann simulations.

The LBM employed here simulates two immiscible fluids which are separated by a definite interface at which a surface tension force acts. When the interface is sharp we are simulating the two-layer model and so we expect internal waves at the interface to be described by Eq. (20) where the surface tension between the two fluids may or may not, depending on the wavelength, have an influence over the behaviour of the wave. If the interface is not sharp but has a finite thickness the density profile around the interface region will be better described by Eq. (24) than the density step approximation. There is, however, a significant difference between the continuous density variation model outlined in section 4 and the binary fluid LBM described in section 2: the former describes a single fluid in which there is a density change produced by an external influence (such as a temperature gradient or salinity change) while the later describes two immiscible fluids separated by an interface which, although finite, supports surface tension forces between the fluids. Internal waves with wavelength $\lambda > 3\lambda_m$ can be considered as being driven solely by gravity since the restoring force imposed on the interface by the surface tension is negligible compared to the gravity/buoyancy forces. Thus, in this situation the nature of the wave motion will be governed predominantly by the density distribution at the

interface; that is the relative density change and the rate at which the change occurs. Any surface tension effects at the interface will be negligible and so we should expect a binary fluid interface to react in the same manner as a single fluid with a continuously varying density, provided the density profile is the same in the interface region. Thus in this regime we expect internal waves simulated using a binary fluid model to mimic internal waves in a region where the density varies continuously. When considering shorter waves with $\lambda < 3\lambda_m$ the effect of surface tension at the interface becomes significant in driving the waves. In this case the binary fluid model can not be considered to simulate a single fluid but rather the interface between two different fluids. Here, provided the interface thickness is small with respect to the wavelength and the fluid depths, we expect a simulated wave to behave as an interfacial wave in a two layer fluid as described by Eq. (20).

6 Internal wave simulations

The aim of the LBM simulations of internal waves performed here is, not only to show that the model is capable of such simulations, but also to measure the wave frequency so that it can be compared with theory for a variety of different wave parameters spanning both pure gravity and gravity-capillary tension waves and also different interface thicknesses. It is therefore important that the initialisation process does not impose a frequency on the system, but rather the oscillation rate is determined solely by the gravitational and surface tension forces. To this end, standing waves were modelled since they can be initialised, using the method described below, in such a way that wave frequency and initial velocity do not need to be estimated. Firstly the values of g_a and g_b are selected to give the desired values of f and g. The interfacial energy, κ, is then selected to give the desired interface properties. Here only two values of κ were used, however, in general

the value of κ can be found for the desired interface. The value of τ_ρ is selected to give the required value of the viscosity. Finally the wavelength is selected; the value of the wavelength relative to λ_m will determine whether the wave is a pure gravity wave or a gravity-capillary wave. In the simulations presented here a grid with λ points in each direction is used. At the top and bottom of the grid a fixed boundary is applied along the $\boldsymbol{e}_2$ direction. At this boundary no-slip boundary conditions are applied which fix the fluid velocity to zero [29]. Periodic boundary conditions are applied at the other two grid edges. Since the fluid evolves on a hexagonal grid the length of these edges is $\sqrt{3}\lambda/2$ so, when the interface is at the centre of the grid, each fluid has depth $h_1 = h_2 = \sqrt{3}\lambda/4$ and $\tanh(kh_1) = \tanh(kh_2) = 0.991$. The grid is then initialised so that $\rho = 1$ and $\boldsymbol{u} = 0$ everywhere and d is +0.5 and -0.5 above and below the centre line respectively. This is done by setting f_i and and g_i equal to their equilibrium values given by Eqs. (3) – (7) and (12) where the derivatives are all set to zero. The value of $d = \pm 0.5$ is taken from figure 2. The simulation is run until the interface and fluid densities settle into their correct forms (for the values of κ, g_a and g_b used). Finally the standing wave is included by shifting each row of the grid by an amount $a\cos(kx)$. Values of f_i and h_i which are shifted off the top and bottom of the grid are disposed of and empty sites, close to the solid boundary, are replaced with their original values. This initialises a standing wave with wavelength λ and amplitude a, at the extreme of its oscillation where the velocity is zero everywhere. The density profile at the interface and the relative densities of each fluid will be correct for the values of κ, g_a and g_b selected due to the first phase of the initialisation process. Once the first part of the procedure has been performed once for parameters κ, g_a and g_b there is no need to repeat it for simulations with different wavelengths. This procedure insures that the standing wave is initialised correctly for the parameters being used without any need to calculate the expected frequency or wave

velocity at the initial time. Any motion which arises will be driven by the surface tension force acting at the interface and the gravity/buoyancy force.

7 Simulated wave frequencies

Standing internal waves were simulated using the binary fluid LBM for the two interfacial energies considered above. For each of the simulations the height of the interface (taken as the height where d is closest to zero) at the antinode was measured at each time-step. This time series was then fitted to a damped co-sine curve to find the wave frequency ω [16]. The dimensionless measured frequency $\Omega = \omega/\omega_0$ is shown in figures 3 and 4 for two values of g_a, the value of g_b is varied to give different values of f. The simulation results are shown for $\kappa = 0.1$ and $\kappa = 0.001$ and the curves are ω_2/ω_0 for the corresponding values of σ and ω_c/ω_0 when $l = 10$. In figure 3 the results for $\kappa = 0.001$ correspond to pure gravity waves since $\lambda/\lambda_m > 8.87$ for the values of f used. The results for $\kappa = 0.1$ correspond to interfacial waves where gravity and surface tension both have an influence over the frequency since here $1.22 < \lambda/\lambda_m < 2.33$. In both cases the results show good agreement with the predictions of the two-layer model although the measured frequency is always slightly smaller than the theoretical frequency. This is probably due to higher order terms in the viscosity being neglected or to a small bias in the curve fitting procedure. The results for $\kappa = 0.1$ show no agreement with the continuous density gradient model despite the continuous change in density over the relatively wide interface. However, the interfacial tension is significant here with respect to gravity ($\lambda/\lambda_m < 3$), so we can conclude that the action of surface tension is producing an interface with the properties of a two-layer model rather than a continuously varying density. In figure 4 the waves with $\kappa = 0.001$ are also pure gravity waves, $\lambda/\lambda_m > 7.16$. When $\kappa = 0.1$ we have λ/λ_m varying from 0.97 when $f = 1.05$ to 7.38 when $f = 2.0$. The critical ratio $\lambda/\lambda_m = 3$

corresponds to $f = 1.36$. Thus the waves are significantly affected by the surface tension for the lower values of f, however at the higher values of f surface tension has only a small effect. For $f < 1.5$ the results follow the theoretical predictions of the two-layer model with the simulated frequencies slightly smaller than the theoretical frequencies, as was observed in figure 3. When $f > 1.5$ the results for $\kappa = 0.001$ (sharp interface) continue to follow the theoretical prediction of the two-layer model. The results for $\kappa = 0.1$ (wide interface), however, appear to deviate in that they become larger than the predications of the two-layer model and remain approximately constant at a value slightly smaller than that predicted by the continuous density variation model. In this region the simulation results do not fit either curve exactly and many of the measurements are equally close to both curves. However, since the results for the different values of κ do not appear to be merging, as the two-layer curves do, and we might expect the simulation results to be slightly smaller than the theoretical results as observed in figure 3, we can conclude that in regions where surface tension can be neglected the model appears to behave as a single fluid with a continuous density variation over a given width. When surface tension can not be neglected the model behaves as a two-fluid model regardless of the interface thickness. We note that while the range of f in figure 3 is also present in figure 4 the values of the dimensionless frequency, Ω, are different. This is because the ratio of λ/λ_m is different.

Internal wave simulations performed using the LBM model described here have been compared with experimental measurements of internal waves [17] at a fresh water-saline interface. At such an interface there is no surface tension and the interface has a finite, continuous width. It would be of interest to obtain experimental data for internal waves at an immiscible interface for comparison with the simulation results presented here.

One approach to achieve this could be based on the experimental work of Waddell *et al.* [30] where the Rayleigh-Taylor instability is generated between an immiscible system consisting of calcium nitrate dissolved in distilled water and heptane. In this system the surface tension can be altered by adding a surfactant enabling the critical wavelength λ_m is be varied without changing any of the physical dimensions of the experimental apparatus.

8 Conclusion

We have seen that the binary, immiscible LBM incorporating gravity can correctly simulate interfacial waves where surface tension is a significant factor in driving the wave motion. This has been observed for different interface thicknesses. Pure gravity internal waves, where the density varies smoothly over a finite region of depth l, have also been simulated. In this situation, where surface tension forces are negligible compared to gravity, the two-layer nature of the LBM is not a significant factor and the characteristics of the wave are determined solely by the density distribution over the depth l. This was observed with $l/\lambda \simeq 0.04$. This extends the application of the LBM and identifies its range of application. In particular, the model can be applied to simulate interfacial waves at a sharp density step where the motion is driven by surface tension and/or buoyancy. Further, by varying the interfacial energy, κ, a wide fluid interface can be achieved. In this case we have demonstrated, for the first time, that the LBM simulations are consistent with an internal wave in a region of smoothly varying density, provided the wavelength of the wave is sufficiently large that the surface tension effects are negligible.

Acknowledgements

The authors would like to thank the Edinburgh Parallel Computing Centre (EPCC) for providing us with computer resources.

References

[1] S. Chen and G. D. Doolen, Lattice Boltzmann method for fluid flows, *Annu. Rev. Fluid Mech.* **30**, 329–364 (1998).

[2] Y. H. Qian and D. d' Humières and P Lallemand, Lattice BGK models for Navier-Stokes equation, *Europhys. Lett.* **17**, 479–484 (1992).

[3] E. Orlandini, M. R. Swift and J. M. Yeomans, A lattice Boltzmann model of binary-fluid mixtures, *Europhys. Lett.* **32**, 463–468 (1995).

[4] M. R. Swift, E. Orlandini, W. R. Osborn and J. M. Yeomans, Lattice Boltzmann simulation of liquid-gas and binary fluid systems, *Phys. Rev. E* **54**, 5041–5052 (1996).

[5] A. Lamura, G. Gonnella and J. M. Yeomans, A lattice Boltzmann model of ternary fluid mixtures, *Europhys. Lett.* **45**, 314–320 (1999).

[6] X. W. Shan and H. D. Chen, Lattice Boltzmann model for simulating flows with multiple phases and components, *Phys. Rev. E* **47**, 1815-1819 (1993).

[7] H. Chen, B. M. Boghosian, P. V. Coveney and M. Nekovee, A ternary lattice Boltzmann model for amphiphilic fluids, *Proc. R. Soc. Lond. A* **456**, 2043–2057 (2000).

[8] N. S. Martys and J. F. Douglas, Critical properties and phase separation in lattice Boltzmann fluid mixtures, *Phys. Rev. E* **63**, 031205-1–18 (2001).

[9] D. Halpern, Observations on short-period internal waves in Massachusetts Bay, *J. Mar. Res.* **29**, 116–132 (1971).

[10] L. R. Haury, M. G. Briscoe and M. H. Orr, Tidally generated internal wave packets in Massachusetts Bay USA.: Preliminary physical and biological Results, *Nature* **278**, 312–317 (1979).

[11] A. R. Osborne and T. L. Burch, T. L. Internal solitons in the Andaman Sea, *Science* **208**, 451–460 (1980).

[12] D. M. Farmer and J. D. Smith, Tidal interaction of stratified flow with a sill in Knight Inlet, *Deep Sea Res. A* **27**, 239–254 (1980).

[13] Q. Zheng, V. Klemas and X.-H. Yan, Dynamic interpretation of space shuttle photographs: deepwater internal waves in the Western Equatorial Indian Ocean, *J. Geophys. Res.* **100**, 2579–2589 (1995).

[14] A. S. Kuznetsov, A. N. Paramonov and Y. A. Stepanyants, Investigation of solitary waves in the Tropical zone of the Western Atlantic, *Atmos. Oceanic Phys.* **20**, 840–846 (1984).

[15] A. Osborne, T. Burch and R. Scarlet, The influence of internal waves on deep water drilling, *J. Petroleum Technol.* **30**, 1497–1509 (1978).

[16] J. M. Buick and C. A. Greated, Lattice Boltzmann modeling of interfacial waves, *Phys. Fluids* **10**, 1490–1511 (1998).

[17] J. M. Buick, A. J. Martin, J. A. Cosgrove, C. A. Greated and W. J. Easson, Comparison of a lattice Boltzmann simulation of steep internal waves and laboratory measurements using particle image velocimetry, *European Journal of Mechanics B/Fluids* **22**, 27–38 (2003).

[18] R. P. Fedkiw, T. Aslam, B. Merriman and S. Osher, A non-oscillatory Eulerian approach to interfaces in multimaterial flows (the Ghost Fluid Method), *J. Comp. Phys.* **152**, 457–492 (1999).

[19] R. P. Fedkiw, T. Aslam and S. Xu, The Ghost Fluid Method for deflagration and detonation discontinuities, *J. Comp. Phys.* **154**, 393–427 (1999).

[20] H. Shouxin, Y. Guangwu and S. Weiping, A lattice Boltzmann model for compressible perfect gas, *Acta Mechanica Sinica* **13**, 218–226 (1997).

[21] J. M. Buick and C. A. Greated, Gravity in a lattice Boltzmann model, *Phys. Rev. E* **61** 5307–5320 (2000).

[22] V. M. Kendon, M. E. Cates, I. Pagonabarraga, J. C. Desplat and P. Bladon, Inertial effects in three-dimensional spinodal decomposition of a symmetric binary fluid mixture: a lattice Boltzmann study, *J Fluid Mech.* **440** 147–203 (2001).

[23] J. Lighthill, *Waves In Fluids,* Cambridge University Press (1978).

[24] J. Turner, *Buoyancy Effects In Fluids,* Cambridge University Press (1973).

[25] A. Defant, *Physical Oceanography,* Pergamon Press, volume II (1961).

[26] W. J. Harrison, The influence of viscosity on the oscillations of superposed fluids, *Proc. Lond. Math. Soc. Series 2* **6**, 396–405 (1908).

[27] O. M. Phillips, *The Dynamics of the Upper Ocean,* Cambridge University Press (1969).

[28] R. Courant and D. Hilbert *Methods in Mathematical Physics,* Interscience (1953).

[29] D. R. Noble, S. Chen, J. G. Georgiadis and R. O. Buckius, A consistent hydrodynamic boundary condition for the lattice Boltzmann method, *Phys. Fluids* **7**,

203–209 (1995).

[30] J. T. Waddell, C. E. Niederhaus and J. W. Jacobs, Experimental study of Rayleigh-Taylor instability: Low Atwood number liquid systems with single-mode initial perturbations, *Phys. Fluids* **13**, 1263–1273 (2001).

Figure 1: The density, along a line through the centre of a bubble, as a function of position x. The centre of the bubble is at $x = 32$. The density profile across the interface can be seen for the two values of the interfacial energy κ considered in this paper.

Figure 2: The order parameter, along a line through the centre of a bubble, as a function of position x. The centre of the bubble is at $x = 32$. The change in the order parameter across the interface can be seen for two values of the interfacial energy κ considered in this paper. Also shown is the curve for $\kappa = 0.2$ to allow direct comparison with [4]

Figure 3: The dimensionless measured frequency Ω as a function of f for $\kappa = 0.001$ and $\kappa = 0.1$ when $g_a = 0.00005, \nu = 0.05$ and $\lambda = 256$. Also shown are the theoretical frequencies ω_2/ω_0 and ω_c/ω_0 for a viscous two-layer model and an inviscid model with a continuous density change over an interface with width $l = 10$.

Figure 4: The dimensionless measured frequency Ω as a function of f for $\kappa = 0.001$ and $\kappa = 0.1$ when $g_a = 0.0001, \nu = 0.05$ and $\lambda = 256$. Also shown are the theoretical frequencies ω_2/ω_0 and ω_c/ω_0 for a viscous two-layer model and an inviscid model with a continuous density change over an interface with width $l = 10$.

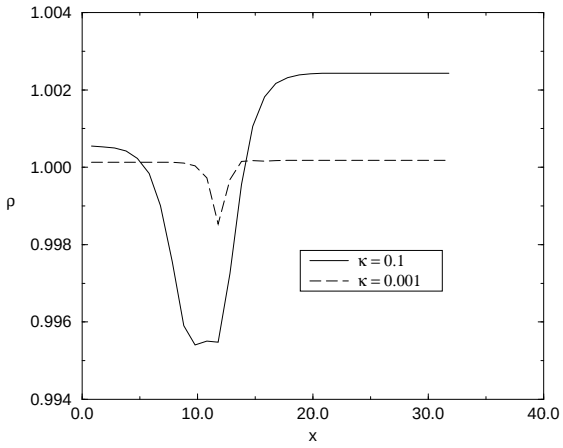

Buick *et al.* Figure 1

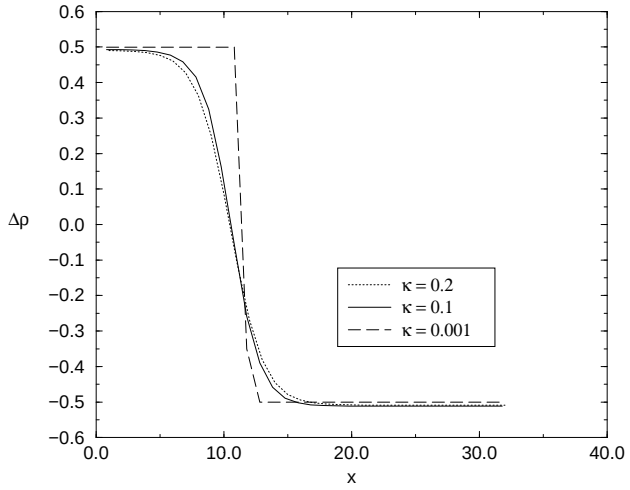

Buick *et al.* Figure 2

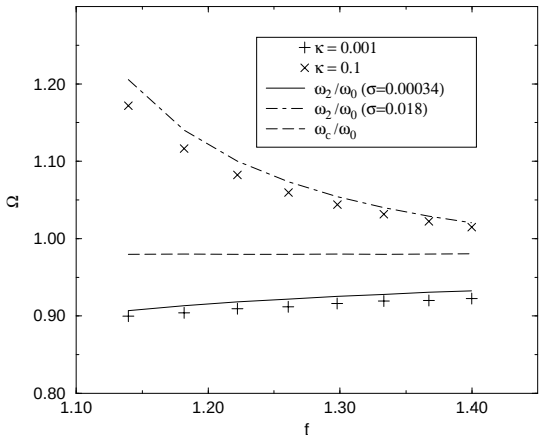

Buick *et al.* Figure 3

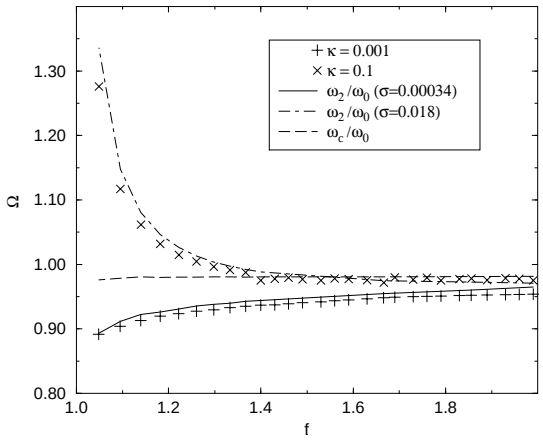

Buick *et al.* Figure 4